Numerical existence and stability
of solutions to the distributed
spruce budworm model

Hala Al-Khalil, Catherine Brennan, Robert Decker,
Aslihan Demirkaya and Jamie Nagode

msp

msp

Numerical existence and stability of solutions to the distributed spruce budworm model

Hala Al-Khalil, Catherine Brennan, Robert Decker, Aslihan Demirkaya and Jamie Nagode

(Communicated by John Baxley)

This paper presents the steady-state solutions and traveling wave solutions for a spatially distributed PDE version of the spruce budworm model. The ODE (undistributed) model has been used in practical scenarios to model the outbreaks of the spruce budworm in forest environments, alongside the study of concepts involving fixed points and bifurcations in introductory differential equations courses. This study represents the spread of an outbreak from one end of a forest to the other. Numerical simulations are conducted using spectral methods.

1. Introduction

In the early 1900s, regions of eastern Canada began to see periodic outbreaks in the spruce budworm population, occurring approximately forty years apart [Williams and Birdsey 2003]. These outbreaks caused severe forest devastation, particularly in conifer tree species that are preferred by the budworms. In response to these population explosions, researchers at the University of British Columbia sought to explain and predict the outbreaks using mathematical models. The spruce budworm model, introduced in [Ludwig et al. 1978], is a modified logistic growth equation with an additional term, $p(N)$, to account for budworm mortality due to predation. Specifically,

$$\frac{\mathrm{d}N}{\mathrm{d}\tau} = r_B N\left(1 - \frac{N}{K_B}\right) - p(N) \quad \text{with} \quad p(N) = \frac{BN^2}{A^2 + N^2}, \qquad (1)$$

where N represents the spruce budworm population, r_B represents the intrinsic growth rate and K_B is the carrying capacity of the budworm population. The predation term $p(N)$ is determined by the *switching value A* and the predation efficiency B. The switching value for predation refers to the minimum budworm

population required to cause birds to take interest in them as a source of food. Predation efficiency refers to the degree of accuracy exhibited by predatory birds in the capture of budworms.

Equation (1) contains variables of varying dimensions, making numerical analysis a challenge. To simplify (1), we seek to remove physical dimension from the variables. Substituting

$$u = N/A, \quad r = Ar_B/B, \quad q = K_B/A, \quad \text{and} \quad t = B\tau/A$$

into (1), we find the nondimensionalized spruce budworm model

$$\frac{du}{dt} = ru\left(1 - \frac{u}{q}\right) - h(u) \quad \text{with} \quad h(u) = \frac{u^2}{1+u^2}, \tag{2}$$

where u represents the budworm population density and t represents time. As with the logistic growth model, r and q correspond with the natural growth rate and the carrying capacity of the population respectively.

The traditional spruce budworm model simulates a stationary population over time. It does not account for the spatial layout of the budworm habitat or the diffusion of the population across this habitat. In order to make the spruce budworm model mimic a diffusive insect population, the addition of a diffusion term is necessary. The fundamental differential equation of diffusion in one spatial dimension x is given by

$$C_t = aC_{xx},$$

where C is the concentration of the diffusing substance, t is the time variable, x is the spatial variable and a is the diffusion coefficient. The term C_t represents the change in the concentration of the diffusing substance with respect to time, and the term C_{xx} accounts for the diffusing substance changing over space, or along the x axis. Making use of Fick's second law of diffusion, we can deduce that the diffusion of the spruce bud worm population u across a linear habitat defined by x can be modeled by the second derivative of u in respect to x. The addition of the diffusion term au_{xx} to (2) leaves us with the distributed spruce budworm model

$$u_t = au_{xx} + ru\left(1 - \frac{u}{q}\right) - \frac{u^2}{1+u^2}, \tag{3}$$

which simulates a migratory population that is both time and space-dependent.

In this paper, we study the numerical existence of the steady-state and the traveling wave solutions of (3). First we use the shooting method to determine the steady-state solutions at various diffusion rates (a) and identify bifurcation values that produce additional steady-state solutions. Then we vary the carrying capacity values (q) and determine the growth rate (r) where the traveling solutions travel to the right, to the left or stay there without a movement, and numerically estimate the velocities

for various combinations of r and q. Finally, we study the relation between the carrying capacity and the growth rate for various values of traveling velocities.

2. Numerical methods and the region of exploration

2.1. *Numerical methods.* We use numerical methods to compute and simulate the steady-state and traveling wave solutions of (3). We discretize in the spatial (x) direction, and use a spectral differentiation matrix D_{xx} as in [Trefethen 2000] to approximate u_{xx} as $D_{xx}u$. This turns the PDE into a system of ODEs. We then use the shooting method along with the Matlab fsolve command to identify the steady states. Spectral differentiation matrices were paired with Matlab's built in ODE solver ode45 to form a PDE solver that we used to verify steady-state solutions found from the shooting method and fsolve, and to simulate traveling wave solutions. The spatial range is chosen to be $-1 \le x \le 1$.

2.2. *Parameter ranges of exploration.* As the carrying capacity value q, growth rate r and diffusion constant a vary, the number of steady states and traveling waves of (3) changes. First we find the steady-state solutions (fixed point solutions) of the undistributed system (2) which satisfy the equation

$$ru\left(1 - \frac{u}{q}\right) = \frac{u^2}{1 + u^2}. \tag{4}$$

Since (4) can be written as a quartic equation, we expect a maximum of four solutions. Our interest is the case where four fixed solutions exist. In order to find these solutions, we look for the intersection points of the two functions

$$y_1 = ru\left(1 - \frac{u}{q}\right) \quad \text{and} \quad y_2 = \frac{u^2}{1 + u^2}.$$

In Figure 1, upper left, we present the intersection points of these two function curves when $r = 0.5$ and $q = 10$. Clearly $u = 0$ is a solution, so we have divided both y_1 and y_2 by u and graphed both functions to visualize the other three intersection points. For these values, the corresponding fixed point solutions are $u = 0$, $u = 0.6834$, $u = 2.0000$ and $u = 7.3166$. In Figure 1, upper right, for these q and r values, we show the corresponding direction field of (2). As shown in this direction field, $u = 0.6834$ and $u = 7.3166$ are stable solutions, while $u = 0$ and $u = 2.0000$ are unstable solutions. In Figure 1, lower left and lower right, we present q and r values (on different scales) that gives us four intersection points of the two curves y_1 and y_2, i.e., the four fixed solutions of (2).

When there are four solutions to (4), the solution $u = 0$ will always be one of them, and it will be unstable. The smallest nonzero solution we will refer to as the "refuge level" and the largest nonzero solution as the "outbreak level", which are

both stable. Between these two stable equilibria is an unstable one that we will refer to as "intermediate".

As the carrying capacity q gets larger, the range of r values that provide four intersection points approaches $0 < r < 0.5$. To show this, consider (4) and then let $q \to \infty$. This results in a cubic equation in u, with $u = 0$ being one of the roots. The discriminant of the resulting quadratic equation (after $u = 0$ is factored out) is $-4r^2 + 1$, and hence to get three solutions (the fourth has gone to infinity) we require $0 < r < 0.5$, assuming positive r. The smallest value of q for which there are four intersection points is about $q = 5$.

Until now we only considered the fixed point solutions of the nondistributed model (2) and found q and r values that give us the maximum number of fixed point solutions (and hence two stable equilibria). We might expect that these q and r values would also give us two stable steady-state solutions (refuge and outbreak) to the distributed model and perhaps the maximum number of steady states of the distributed model (3). In fact we will see that as a, the diffusion constant, gets smaller, the number of steady states gets bigger. Also, the existence of the refuge and outbreak steady states are a dependent.

Finally, we use a values in the range $0.0005 < a < 0.1$. This range includes a values appropriate to both steady-state and traveling wave solutions that illustrate our findings.

3. Steady state solutions

In this section we will present the numerical steady-state solutions of (3) with the boundary conditions

$$u(-1, t) = 0, \quad u(1, t) = 0. \tag{5}$$

As we discussed in Section 2.2, we are interested in q and r values that will provide us the maximum number of steady-state solutions for the nondistributed case. For this purpose we now illustrate our results for $r = 0.5$ and $q = 10$.

Steady state solutions $u(x, t) = \phi(x)$ to (3) do not change over time, i.e., $\phi_t = 0$. Thus ϕ satisfies the following ordinary differential equation:

$$0 = a\phi'' + r\phi\left(1 - \frac{\phi}{q}\right) - \frac{\phi^2}{1 + \phi^2}, \tag{6}$$

with $\phi(-1) = 0$ and $\phi(1) = 0$. We can change this second-order differential equation into a first-order system by defining $y_1 = \phi$ and $y_2 = \phi'$. Then we get the system

$$y_1' = y_2, \quad y_2' = \frac{-ry_1}{a}\left(1 - \frac{y_1}{q}\right) + \frac{y_1^2}{a(1 + y_1^2)}. \tag{7}$$
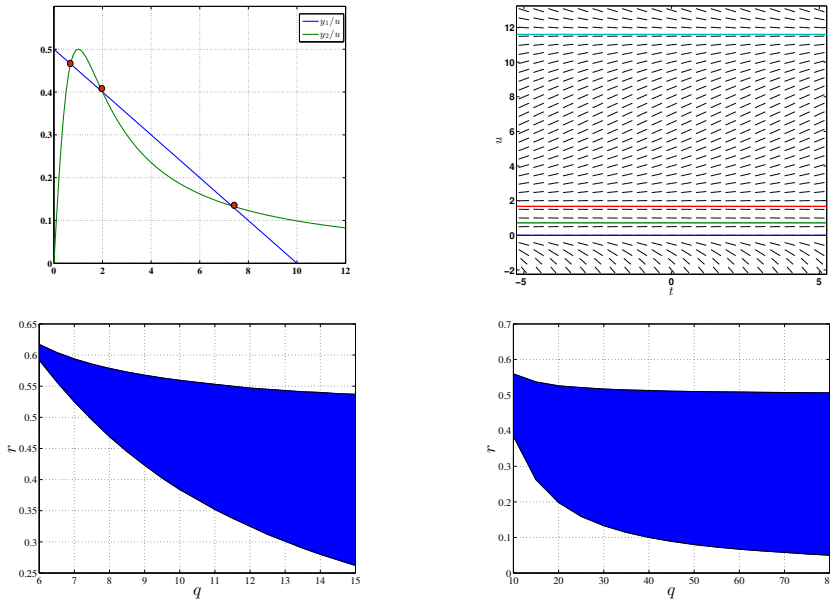
Figure 1. Upper left: the nonzero intersections of y_1 and y_2 occurs at $u = 0$, $u = 0.6834$, $u = 2.0000$ and $u = 7.3166$ when $r = 0.5$ and $q = 10$. Upper right: the direction field of the nondistributed model (2) when $r = 0.5$ and $q = 10$. Lower left and lower right: r vs. q values that gives exactly four fixed point solutions to (2).

A phase portrait of the system of equations (7) is shown in Figure 2, for $r = 0.5$, $q = 10$ and $a = 0.1$. Other a values give a similar phase portrait (with a different scale on the y axis). In the phase portrait, one can see the four fixed points for the undistributed model, now as centers and saddles. The first (a center) is at the origin, the second (a saddle) is at $\phi = 0.6834$, the third (a center) is at $\phi = 2$ and the fourth (a saddle) is at $\phi = 7.3166$.

3.1. *The shooting method.* The shooting method is a numerical technique for solving two-point boundary value problems (BVP's) by reformulating them as initial value problems (IVP's). The objective of this method is to determine initial conditions for the corresponding IVP that produce solutions that satisfy the original BVP. Solutions are found by fixing the left boundary point of the solution and guessing the initial slope until the right-hand boundary condition is satisfied.

Several sample solutions to (6) on $[-1, 1]$ with initial conditions $\phi(-1) = 0$ and $\phi'(-1) = \omega$ are plotted in Figure 3. The value of ω, or the initial slope of the solution, is varied until the right endpoint of the solution, $\phi(1)$, meets the desired boundary value at zero.
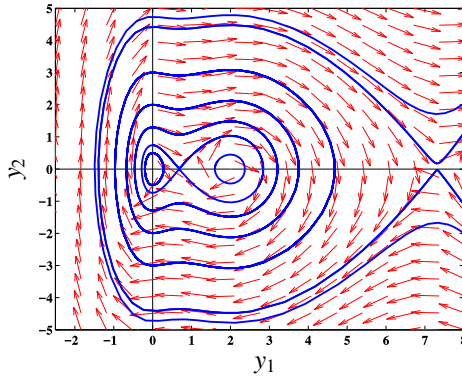
Figure 2. Phase portrait of (7) when $a = 0.1$, $r = 0.5$ and $q = 10$.
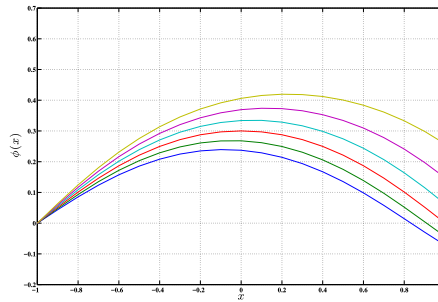

Figure 3. Solutions to the IVP (bottom to top) $\omega = 0.44$, 0.48, 0.52, 0.56, 0.60 and 0.64 and for $r = 0.5$, $q = 10$ and $a = 0.1$.
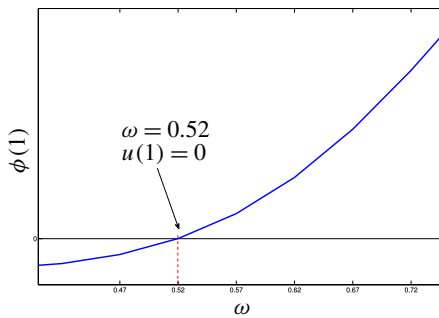

Figure 4. The solution $\phi(1)$ as a function of ω for $r = 0.5$, $q = 10$ and $a = 0.1$.

A plot of the right endpoints $\phi(1)$ versus the initial slope values ω can be used to determine the appropriate initial conditions to produce a solution to (6); see Figure 4. When the $\phi(1)$ vs. ω curve intersects the ω axis, $\phi(1) = 0$ and the right

boundary condition is met. Each value of ω that causes $\phi(1) = 0$ represents a steady-state solution. Similar results apply to other a values.

3.2. Steady states for various a values. In Figure 5 we show all nonzero steady-state solutions superimposed for a few a values. Solid lines represent stable steady-states, and dashed, dotted or dash-dot lines represent unstable ones.

The steady states for each diffusion rate, or a value, were determined using both the shooting method and the phase portrait of (7), which is shown in Figure 2. Within the shooting method plots, we expect a new steady-state solution to emerge each time the ω axis is intersected. Furthermore, the ω value at the point of intersection corresponds with the initial slope of the equilibrium solution. The phase portrait helps to make sure that no steady-state solutions are missed; each steady-state solution must start on the ϕ' axis and end on the ϕ' axis ensuring that $\phi = 0$ at $x = -1$ and $x = 1$, as required by the boundary value problem.

At $a = 0.05$, there are two positive initial conditions that force the boundary condition at $\phi(1)$ to meet zero: $\omega \approx 0.19$ and $\omega \approx 0.97$. In Figure 6, left, we see these values as points where the shooting plot crosses the ω axis, and in Figure 6, right, we see these values as the starting values of the phase plots of the steady-state

$a = 0.05$

$a = 0.0225$

$a = 0.02$

$a = 0.0125$
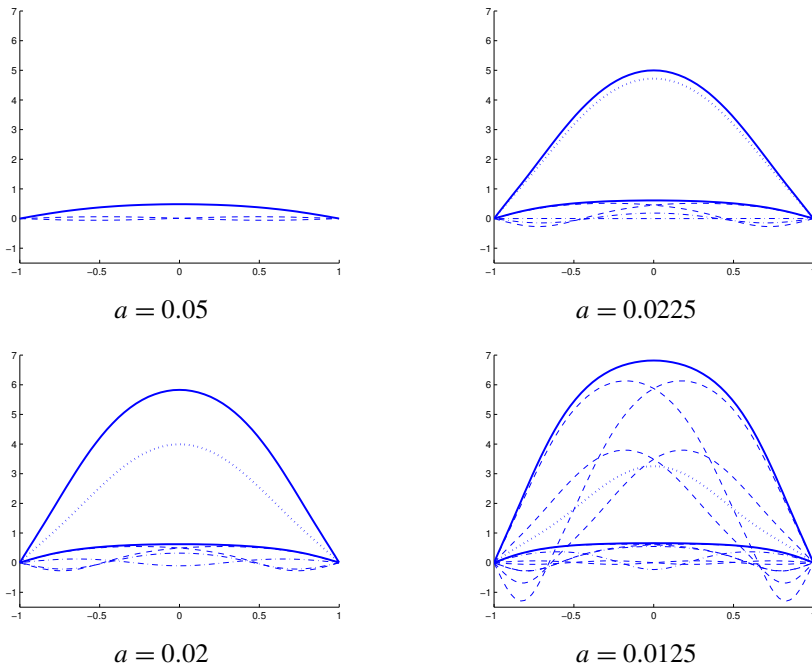
Figure 5. Nonzero steady-state solutions for several a values and for $r = 0.5$ and $q = 10$.

$\phi'(-1)$ vs. $\phi(1)$ ϕ' vs. ϕ
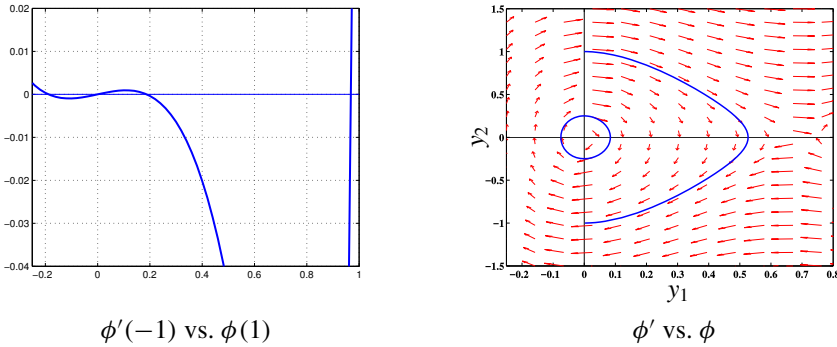
Figure 6. Steady-state solutions for $a = 0.05$, $r = 0.5$ and $q = 10$.

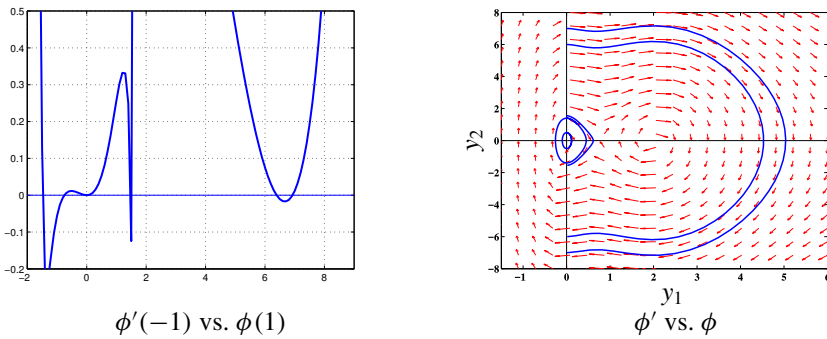$\phi'(-1)$ vs. $\phi(1)$ ϕ' vs. ϕ

Figure 7. Solutions for $a = 0.0225$, $r = 0.5$ and $q = 10$.

solutions. For the smaller ω-value, the phase plots overlap themselves and thus appear to form a closed loop. Finally, if the initial slope is $\omega \approx -0.19$, we get another steady-state solution, and the phase plot is indistinguishable from the one for which $\omega \approx 0.19$.

Looking back to Figure 5, upper left, we again see the three (nontrivial) steady-state solutions. The one with the larger positive initial slope ($\omega \approx 0.97$) is stable and corresponds to the refuge level of the undistributed model. The unstable solution with the smaller positive initial slope corresponds to the unstable (dashed) solution that goes from slightly positive (on the left) to slightly negative (on the right). The third unstable solution has initial slope $\omega \approx -0.19$ and is a mirror image (left-right) of the other unstable solution.

We now look at what happens when a is lowered to $a = 0.0225$. In Figure 7, right, we find two new solutions whose phase plots wrap around the saddle at $\phi = 0.6834$ and the center at $\phi = 2.000$. This indicates the appearance of a stable outbreak equilibrium solution, and a slightly smaller unstable intermediate steady-state solution, as shown in Figure 5, upper right. At this point we have steady-state

$\phi'(-1)$ vs. $\phi(1)$ ϕ' vs. ϕ
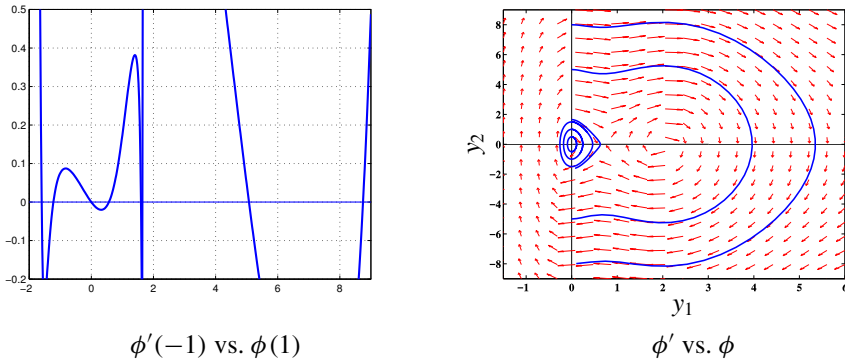
Figure 8. Solutions for $a = 0.02$, $r = 0.5$ and $q = 10$.

solutions corresponding to each of the four fixed points of the nondistributed model, and with similar stability types.

If you look closely at Figure 7, left, it appears that there will be six nonzero equilibrium solutions. There are a pair of positive solutions near $\omega = 1.5$ and another pair of positive solutions near $\omega = 6.65$ (outbreak and intermediate solutions). In addition there are negative solutions near $\omega = -1.5$ and $\omega = -0.75$. Close to zero the situation is not so clear, but upon closer inspection we find another positive solution near $\omega = 0.0055$ (as well as the trivial zero solution).

Three solution types. The solution types can be broken into three groups using phase plots. We define group I as steady-state solutions that start on the positive ϕ' axis and end on the negative ϕ' axis, and form exactly one-half of a loop. These are the solutions that correspond directly to the fixed-points of the nondistributed model, and represent physically realistic solutions. We define group II as solutions that loop around both centers and the smaller saddle one or more times (including half loops such as 1.5 or 2.5 loops). We will also refer to these as "big loops", and they appear as "big waves" in the ϕ vs. x plots of Figure 2. Because these solutions have negative ϕ values, they are not physically realistic. Group III then consists of solutions that loop around only the origin one or more times ("small loops" in the phase plane or "small waves" in the ϕ vs. x plots). These solutions are not physically realistic.

Thus as a changes from 0.05 to 0.0225 there are two bifurcations; there are two new group I steady-state solutions, and two new group III solutions. The group III solutions are 1.5 loop solutions around the origin (one with positive initial slope and one with equal and opposite negative initial slope).

As a is further reduced to 0.02 (Figure 8), the two larger steady-state solutions (stable outbreak and unstable intermediate half loops) grow more distinct and easily perceivable. Also, the shooting plot now shows that the small positive solution,
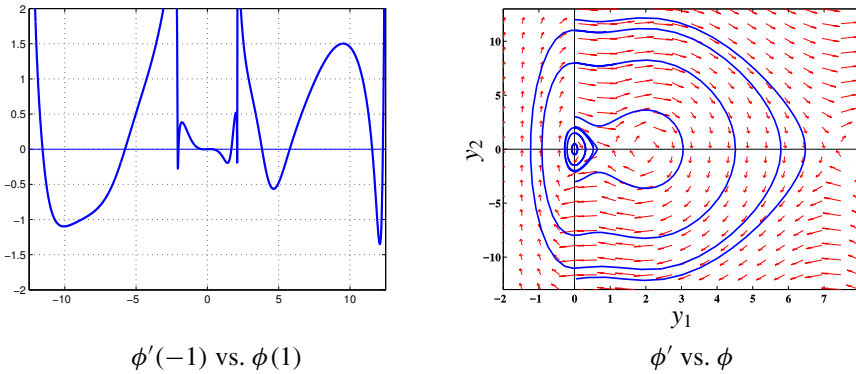
$$\phi'(-1) \text{ vs. } \phi(1) \qquad\qquad \phi' \text{ vs. } \phi$$

Figure 9. Solutions for $a = 0.0125$, $r = 0.5$ and $q = 10$.

which could not be distinguished for $a = 0.0225$, is now clearly visible, and shows up as a loop in the phase plot and a small wave in Figure 2. Thus no bifurcations occur between the a values 0.0225 and 0.02.

Note finally that the two 1-loop inner solutions (one for positive initial slope and one for equal and opposite initial slope) coincide in the phase plane and so cannot be distinguished from each other there. On the other hand, the two 1.5-loop inner solutions (initial slopes positive and negative but not equal and opposite), which are closer to the origin than the 1-loop solutions, are distinguishable in the phase plane.

Finally, when a is lowered again from 0.02 to 0.0125 (see Figure 9), we see two new group II solutions ("big loops" that wrap around once) as well as two group III solutions ("small loops" that wrap around two times). The two small loop solutions have equal and opposite initial slopes, and hence are indistinguishable in the phase plane. Thus two more bifurcations have occurred.

3.3. *Determination of bifurcation values.* [Aron et al. 2014, Theorem 3.4] states that the eigenvalues of the linear boundary value problem

$$\phi'' + \lambda^2 \phi = 0, \quad \phi(-1) = 0, \quad \phi(1) = 0, \tag{8}$$

correspond to the bifurcation values of the nonlinear boundary value problem

$$\phi'' + \lambda^2 (\phi - \phi^3) = 0, \quad \phi(-1) = 0, \quad \phi(1) = 0. \tag{9}$$

The proof is based on the property that close to the origin, the solution curves of the nonlinear problem approach those of the linear one, and that as the solution curves move clockwise around the origin, the ones corresponding to the nonlinear problem move slower (in the sense of the angle in polar coordinates), and are farther from the origin (in the sense of the radius in polar coordinates), than those of the linear problem.
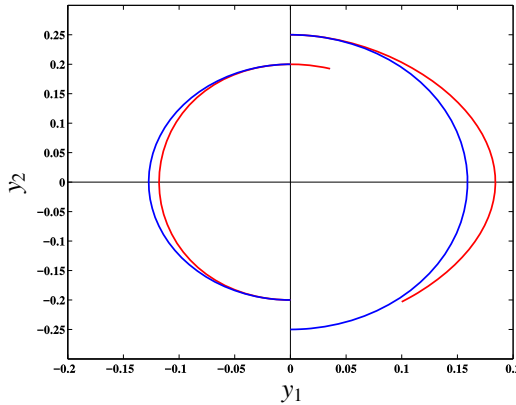
Figure 10. Linear (blue) vs. nonlinear (red) system near the origin.

The spruce budworm BVP (see (6)) can be written as

$$\phi'' + \frac{r}{a}\phi(1-\phi) - \frac{\phi^2}{a(1+\phi^2)} = 0, \quad \phi(-1) = 0, \quad \phi(1) = 0. \tag{10}$$

This equation can also be linearized, giving

$$\phi'' + \frac{r}{a}\phi = 0, \quad \phi(-1) = 0, \quad \phi(1) = 0, \tag{11}$$

which with the identification $\lambda^2 = r/a$ is again (8). We hypothesize that this will give us some of the bifurcation values for the spruce budworm BVP of (10). Solving for a, we have $a = r/\lambda^2$. When $\lambda_n = \frac{1}{2}n\pi$ (eigenvalues from (8)) is substituted into this equation, we find some of the expected bifurcation values of (3) in terms of a:

$$a_n = \frac{r}{\left(\frac{1}{2}n\pi\right)^2} \qquad \text{for} \quad n = 1, 2, 3, 4 \ldots \tag{12}$$

The bifurcations calculated from (12) correspond to the emergence of a new small half loop (for $n = 1$) and new small loops (for $n > 1$) in the terminology of the previous section. That these can be calculated analytically is a result of the linearization of the problem for solution curves near the origin. For bifurcation values corresponding to the emergence of new big loop solutions (group II) we have estimated the bifurcation values using numerical exploration.

Finally, there are bifurcations that lead to new small loop solutions that are not given by (12). This is a result of the lack of left-right symmetry in the vector field for the nonlinear spruce budworm BVP, which leads to the property that solution curves in the phase plane travel faster around the origin (in terms of angle in polar coordinates), and closer to it (in terms of the radius in polar coordinates) than those of the linearized equation for $x < 0$, but slower around the origin (and farther

from it) than those of the linearized equation for $x > 0$, as long as the solution curves are sufficiently close to the origin (see Figure 10).

This allows new solutions to the BVP that start on the negative y axis and end on the positive y axis (1.5 loop, 2.5 loop, etc.) to occur for a values slightly larger than the predicted bifurcations values of (12). Only solutions that start on the negative y axis and end on the positive y axis can "outrun" the corresponding linear solution (since they spend more time in the fast region $x < 0$). Thus a values corresponding to the appearance of these types of solutions are the only inner loop bifurcations that must be calculated using numerical experimentation.

In Figure 11, left, we demonstrate a numerically calculated bifurcation of this type at approximately $a = 0.0230814$. To do this we show the endpoints only (with connecting lines for readability) of solution curves for $a = 0.0230830$ and $a = 0.0230800$, corresponding to several initial conditions along the negative $y = \phi'$ axis. The initial conditions used are labeled in the figure. These endpoints correspond to solutions that wrap around the origin about 1.5 times.

One sees that for $a = 0.0230830$ the solution curves do not reach the y axis, and hence they are not solutions to the BVP. For $a = 0.0230800$ the longer curves pass the y axis and the shorter ones fall short of it, showing that there are exactly two new solutions to the BVP. At some point in between these two cases there must be an a value for which the longest solution curve just touches the y axis (this value is about $a = 0.0230814$).

This type of bifurcation is similar to a saddle-node bifurcation for a first-order ordinary differential equation, where at the bifurcation point a single fixed point appears where there was previously none, then this single fixed point splits into two fixed points which grow farther apart. This is also how new big-loop steady-state solutions are created; they must also be estimated using numerical exploration.

Figure 11, right and bottom, shows the two other types of bifurcation that occur to create new steady-state solutions. Figure 11, right, illustrates the type of bifurcation that occurs at a bifurcation point calculated by (12) when new solutions with a fractional number of loops are created (which corresponds to n odd in (12)). For a just larger than the bifurcation value, one observes a solution with negative initial condition and the zero solution. At the bifurcation value there is just the zero solution, and for a just smaller than the bifurcation value there is the zero solution and solution with positive initial condition. This is somewhat similar to a transcritical bifurcation for first-order ODE's.

Bifurcations of this type occur for a slightly smaller than the type shown in Figure 11, left. Thus as a gets smaller, first two new small loop solutions are created which have negative initial conditions (Figure 11, left), and then shortly after that the negative solution that is closest to zero switches over to become positive (Figure 11, right). The net result is one new solution with negative initial
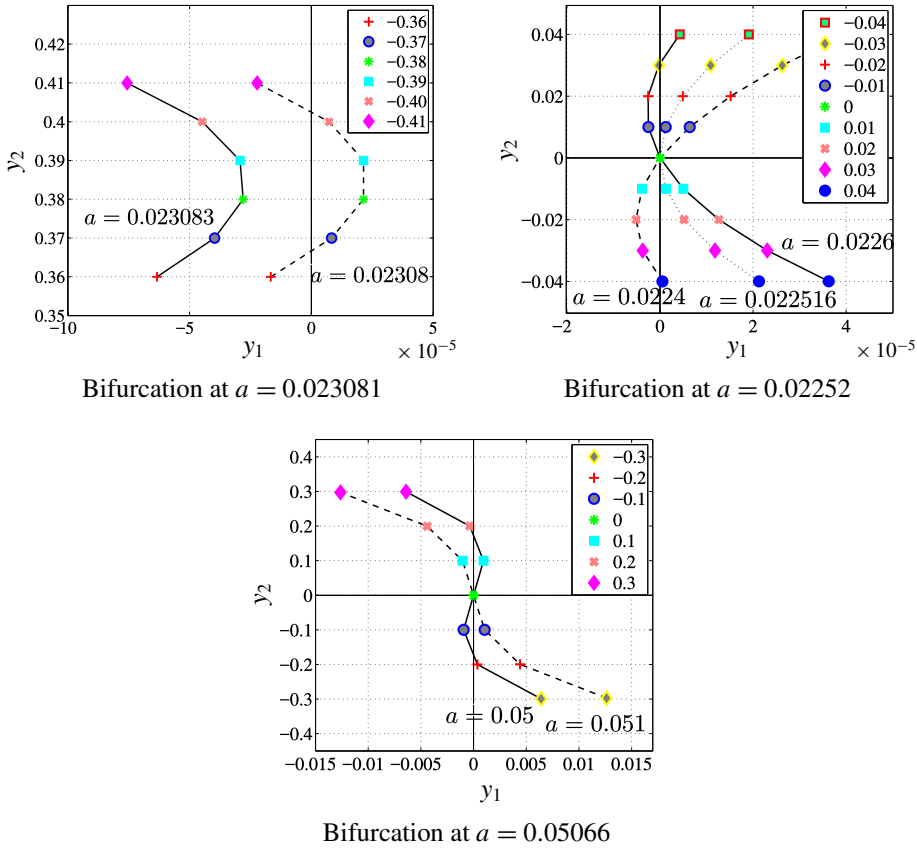
Bifurcation at $a = 0.023081$

Bifurcation at $a = 0.02252$

Bifurcation at $a = 0.05066$

Figure 11. Bifurcation types for $r = 0.5$ and $q = 10$.

condition and one with positive initial condition (in addition to the zero solution) after both bifurcations.

Finally, Figure 11, bottom, shows the type of bifurcation that occurs when new inner loop solutions are created for n even in (12) (nonfractional number of loops). This type of bifurcation can be compared to the pitchfork bifurcation of first-order ODEs; as a is reduced, the zero solution gives rise to two new solutions, one with positive initial condition and one with negative initial condition (the zero solution continues). Note that the end of result of the two bifurcations in Figures 11, left, and 11, right, is similar to the bifurcation in Figure 11, bottom, in that including the zero solution, the number of solutions goes from one to three, corresponding to one new solution with positive initial condition and one negative. The difference is that for the case of even n the initial conditions that correspond to steady-state solutions have equal and opposite sign, but not for the case of odd n.

bifurcation type	bifurcation values in terms of a
small loop from $a_n = r/(\frac{1}{2}n\pi)^2 (n > 1)$	0.05066, 0.02252, 0.01267, 0.00811
small loop estimated numerically	0.023081
small half loop from $a_n = r/(\frac{1}{2}n\pi)^2$ $(n = 1)$	0.20264
big loop estimated numerically	0.0225578, 0.015, 0.0106, 0.0045

Table 1. Bifurcations values for $r = 0.5$ and $q = 10$.

In Table 1 we show all bifurcations that occur for $0.00811 \leq \alpha \leq 0.20264$. From that table we see that the bifurcation just described at $a = 0.023814$ occurs just before (as a gets smaller) the one calculated by (12) at $a = 0.02252$.

3.4. Stability analysis. Our numerical simulations have shown that some of the equilibrium solutions found in Section 3.2 are stable and some are unstable. This has motivated us to check the eigenvalues of the linearized operator of (3) about the steady-state solution ϕ.

Let v be a small perturbation and $u = \phi + v$ the solution to (3), then if we substitute it into (3), we get

$$(\phi + v)_t = a(\phi + v)_{xx} + r(\phi + v)\left(1 - \frac{\phi + v}{q}\right) - \frac{(\phi + v)^2}{1 + (\phi + v)^2}. \quad (13)$$

Since ϕ is a steady-state solution, we have $a\phi_{xx} + r\phi(1 - \phi/q) - \phi^2/(1 + \phi^2) = 0$.
If we linearize the nonlinear terms about the steady-state ϕ, we get

$$v_t = av_{xx} + f(\phi)v,$$
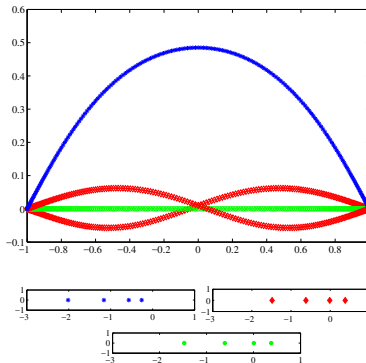
Figure 12. Stable and unstable solutions with color-coded eigenvalue spectrum for $a = 0.05$, $r = 0.05$ and $q = 10$.
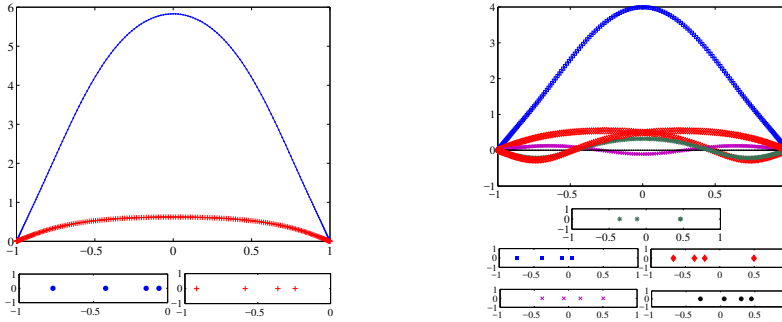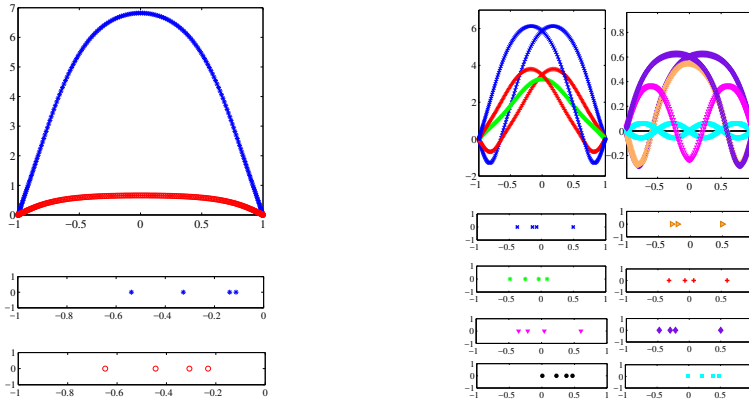
Figure 13. Left: stable solutions with spectrum for $a = 0.002$, $r = 0.5$ and $q = 10$. Right: unstable solutions with spectrum for $a = 0.002$, $r = 0.5$ and $q = 10$.

where

$$f(\phi) = r - \frac{2r\phi}{q} - \frac{2\phi}{(1 + \phi^2)^2}.$$

Then the corresponding linear system is

$$v_t = \mathcal{H}v, \quad \text{where} \quad \mathcal{H} = a\frac{\mathrm{d}^2}{\mathrm{d}x^2} + f(\phi). \tag{14}$$

Our interest is the sign of the real part of the largest eigenvalue of $\mathcal{H}$ for each steady state ϕ. If that value is negative, we expect the perturbation from the steady state to shrink until the perturbed solution conforms to the steady state.

In Figures 12, 13 and 14 we show graphs of the steady-state solutions and the corresponding eigenvalues of $\mathcal{H}$ for the α values 0.05, 0.002 and 0.00125.

In Figure 15 we show snapshots of an animation of a perturbed initial condition and how it converges to a stable steady state. Notice that variations in the initial condition and large deviations from the original steady state do not affect the long term behavior of the solutions. This is typical of the outbreak and refuge solutions, for which all eigenvalues are negative.

Conversely, if the largest eigenvalue has a positive real part, we will expect the perturbation to grow, distancing the perturbed solution from the original steady state; see Figures 16 and 17. Equilibria with positive eigenvalues are unstable and achieved only under specific initial conditions [Seydel 2010]. Subtle changes to an initial condition in the neighborhood of an unstable equilibrium will alter the long term behavior of the solution. Figure 16 shows a small loop solution and Figure 17 shows an intermediate half-loop solution (between outbreak and refuge levels)

In some cases, the perturbed solution will rest near the steady state for a period of time, then slowly gravitate to a new, distinct resting place. This sort of behavior

Figure 14. Left: stable solutions with spectrum for $a = 0.00125$, $r = 0.5$ and $q = 10$. Right: unstable solutions with spectrum for $a = 0.00125$, $r = 0.5$ and $q = 10$.

is typical of equilibria that are "almost stable" in the sense that there is only one positive eigenvalue and it is very small.

4. Traveling wave solutions

We study the traveling wave solutions of (3) that are in the form $u(x, t) = \phi(x - vt)$, where v is the speed of the wave with the boundary conditions

$$u(-1, t) = h, \quad \text{and} \quad u(1, t) = k$$

and the initial condition

$$u(x, 0) = h + \frac{2(k - h)}{\pi} \tan^{-1} e^{Cx}. \tag{15}$$

$$t = 0 \qquad\qquad t = 2 \qquad\qquad t = 10$$
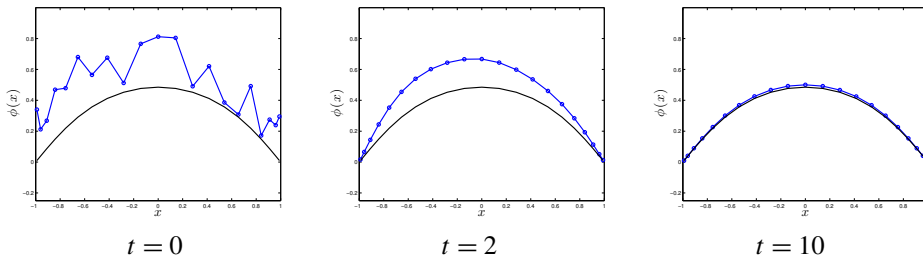
Figure 15. A stable equilibrium solution (printed in black) and a perturbed solution (printed in blue) are plotted each at $t = 0$, $t = 2$ and $t = 10$. The perturbation from the steady state is amplified to highlight insensitivity to changes in the initial condition.

| $t = 0$ | $t = 2$ | $t = 10$ |
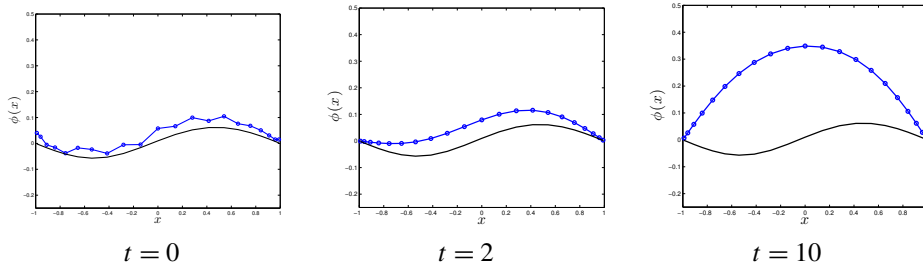
Figure 16. An unstable equilibrium solution (black) and a perturbed solution (blue).

| $t = 0$ | $t = 2$ | $t = 10$ |
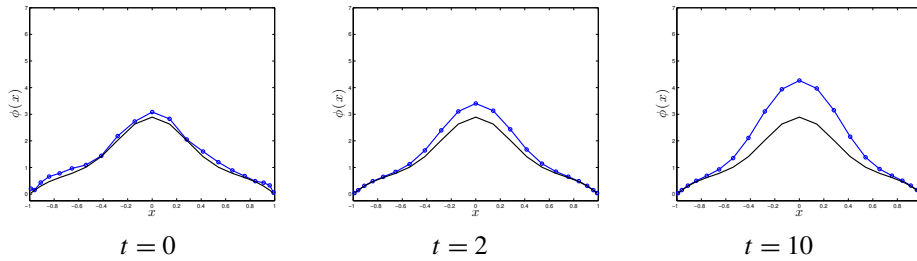
Figure 17. An unstable equilibrium solution (black) and a perturbed solution (blue).

With these boundary and initial conditions (and appropriately chosen C), the solutions are close in shape to traveling wavefronts, and thus quickly converge to traveling wavefronts and end in steady-state solutions. These waves represent growth/decay of the population as a function of the spatial dimension.

4.1. *Choosing boundary conditions.* We pick the boundary conditions as

$$u(-1, t) = h \quad \text{and} \quad u(1, t) = k,$$

where h and k are the fixed point solutions to the nondistributed model (2). As explained in Section 2.2, we consider q and r values that give us the four fixed point solutions to (2). Two of these solutions are stable and the other two are unstable. One of the unstable fixed solutions is the zero solution and if u_{s_1} and u_{s_2} are stable and u_u is the unstable solution, we have the following inequality:

$$0 < u_{s_1} < u_u < u_{s_2}. \tag{16}$$

We are interested in the traveling waves that converge to stable fixed point solutions at ± 1, i.e., $h = u_{s_1}$ and $k = u_{s_2}$.

4.2. *Results.*

4.2.1. *The movement of the wavefront.* Traveling wavefronts move according to the boundary conditions, growth constant r and carrying constant q. Fixing q and varying r, a critical $r = r*$ was found at different q values such that:

- for $r < r*$, the wave travels to the right, and the population dies out;
- for $r > r*$, the wave travels to the left, and infestation occurs;
- for $r = r*$, the wave does not travel, and no population growth or decay occurs.

The behavior of the wave movement was observed after incrementally selecting the values of q from [9, 15] with the increment 1 while r values were varied continuously within an interval for which both the refuge and outbreak levels existed. The effect of changing r and q over a selected range, with $a = 0.001$ fixed, is recorded in Table 2. When the wave moves to the right, it means that the wave favors moving to the refuge solution and the population decreases. On the other hand, the wave favors outbreak and an increase in population when it moves to the left. This behavior is presented in Figure 18 for $a = 0.001$ and $q = 14.5$, with r changing in value from its lowest to highest value within the range of r specified within the four solutions case for (2) as shown Figure 1, lower left. In Figure 18 the wave is plotted at the critical r value where the wave does not move and the thus the population does not change in time.

Note that for a wavefront that starts at the outbreak level on the left and ends at the refuge level on the right, the movement of the wavefront would be in the opposite direction of that just described.

It can be shown that for $a = 1$ that there is an integral condition [Murray 2005] that determines the value of r^* for fixed q for which the velocity is zero. The condition is

$$\int_{u_{s_1}}^{u_{s_2}} ru\left(1 - \frac{u}{q}\right) - \frac{u^2}{u^2 + 1} \, du = 0. \tag{17}$$

In fact, by inspecting the proof in the reference just given, it is clear that this condition works for all positive a values. This condition was checked against the numerically calculated values in Table 2, and the results were consistent. This

q	9	10	11	12	13	14	15
r^*	0.4605	0.4258	0.3956	0.3692	0.3459	0.3252	0.3067

Table 2. Critical r^* that represents zero velocity wavefronts for different q values, calculated numerically for $a = 0.001$, but valid for other a values. Larger r means wavefront moves left (outbreak level increasing) and for smaller r wavefront moves right (outbreak level decreasing).

no movement

moves to the left

moves to the right
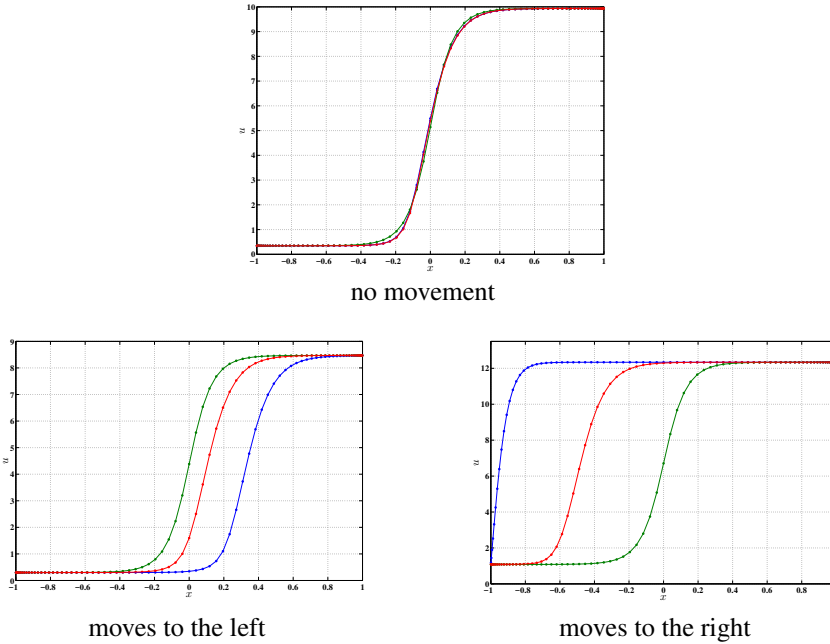
Figure 18. The plots captured at $t = 0$ (blue curve), $t = 5$ (red curve) and $t = 10$ (green curve) with $a = 0.001$ and $q = 14.5$. Top: $r = 0.3165$, $h = 0.345918$ and $k = 9.93485$. Left: $r = 0.28$, $h = 0.2987$ and $k = 8.47012$. Right: $r = 0.538$, $h = 1.03008$ and $k = 12.3281$.

means that even though the values given in Table 2 were calculated with $a = 0.001$, they are valid for other a values.

4.2.2. *Velocity as a function of r and q, with a fixed.* We have studied how the velocity of a traveling wave depends on r and q. Figure 19 shows that relation for a few different values of a. For these charts, the speed was calculated via simulation of the PDE for various r and q values, and then a contour plot of the data was created using Matlab.

These charts can be used to estimate the speed at which an outbreak spreads within the parameter ranges shown.

4.2.3. *The approximately linear relation between v and r, with q and a fixed.* For a fixed q value, by utilizing the ranges of velocities for each q and range of r, we observed an approximately linear relation between r and v. Thus, for a fixed carrying capacity, we can estimate the velocity of the budworm wave as a function of the growth rate of the insect. Figure 20 shows this relation for different values
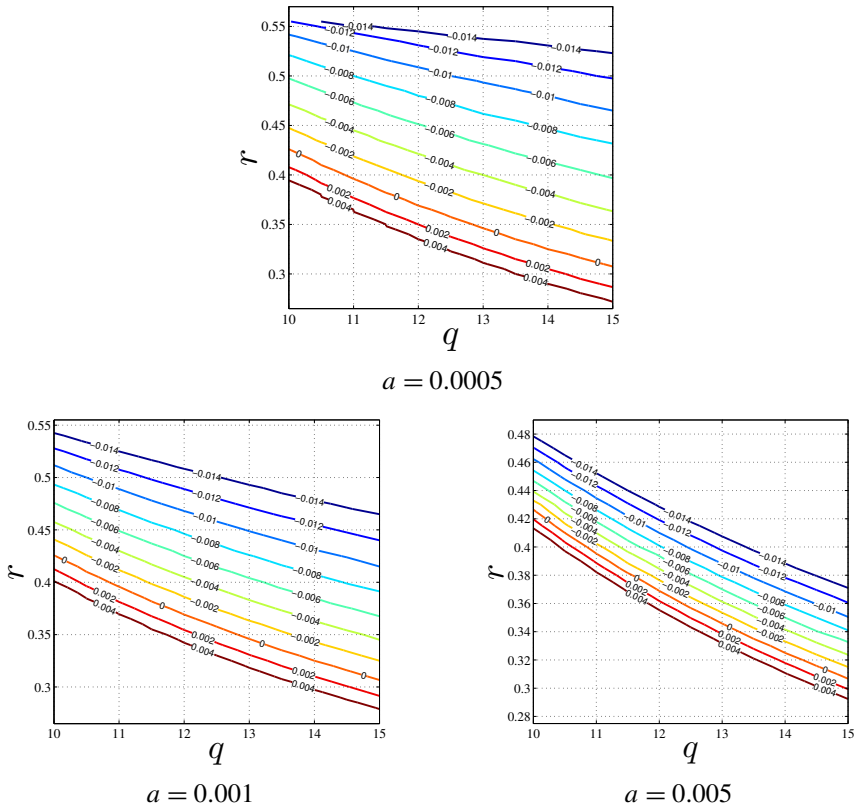
$a = 0.0005$

$a = 0.001$

$a = 0.005$

Figure 19. The speed contour plots.

of q when $a = 0.0005$ and when $a = 0.001$. These equations are consistent with
Figure 19.

5. How outbreaks spread

In this section we demonstrate one possible way for an outbreak of budworms
localized in space can spread to the entire forest (the region $-1 \leq x \leq 1$). We
choose $r = 0.5$ and $q = 10$ again, so that we are in the $r - q$ region where there are
four fixed points. We also choose $a = 0.0005$ which makes sure that the outbreak
and subsistence levels occur in the distributed model as well.

We show how a large enough perturbation of the steady-state solution that
represents the subsistence level of budworms can create a traveling wavefront of the
type studied in the last section, and end in the steady-state solution that represents
the outbreak level. The speed of the wave can be estimated using the charts and
equations from that last section as well.
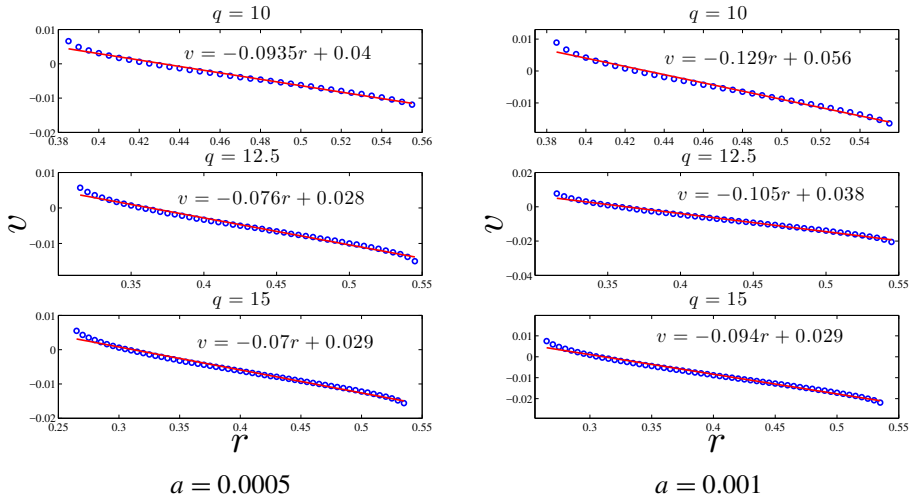
Figure 20. Graphs of r vs. v for fixed q and a.
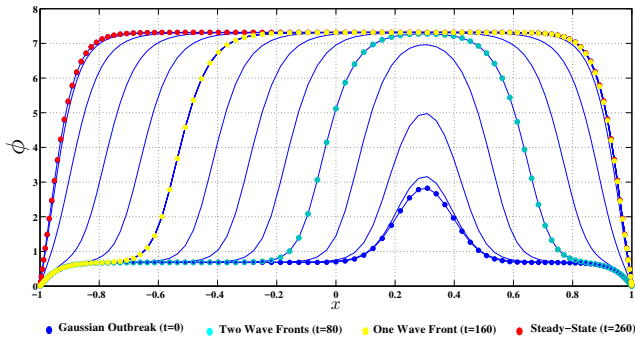
Figure 21. Initial Gaussian increase in budworm population from subsistence level spreads to outbreak.

In Figure 21 we show the effect of imposing a Gaussian bump, representing a small normally distributed increase in the budworm population, on top of a steady-state subsistence solution. In that figure we see snapshots of an animation every 20 time units, starting at $t = 0$ (blue dots). Also highlighted are the times $t = 80$ (cyan dots), $t = 160$ (dark green dots) and $t = 260$ (red dots). The snapshot at $t = 80$ represents the point at which the initial disturbance to the subsistence level has grown so that the top has reached the outbreak level. At this point there are two wavefronts of the type described in Section 4 (one moving left and one moving right) as well as two regions that conform to the steady-state subsistence level ($-1 \leq x \leq -0.2$ and $0.8 \leq x \leq 1$) as described in Section 3.

At $t = 160$ there are three regions; for $-0.25 \le x \le 1$ we observe the population conforming to the steady-state outbreak level of Section 3, for $-0.75 \le x \le -0.25$ we have a traveling wavefront as in Section 4, and for $-1 \le x \le -0.75$ the population conforms to the steady-state subsistence level of Section 3. Finally at $t = 260$ the population has completely reached the steady-state outbreak level.

Finally, from Figure 19 we can estimate the speed of the wavefront to be slightly larger than -0.006 (for the left-moving front); the equation from Figure 20, right, gives -0.0067. In the 80 time units that separate the snapshots at $t = 80$ and $t = 160$ we would expect the wavefront to move about -0.5 units to the left, which is what is seen in Figure 21.

6. Conclusion

The original spruce budworm model is an ordinary differential equation and it models the outbreaks of the spruce budworm in forest environments. By adding the diffusion term au_{xx} to the original equation, we got the distributed model, which is a partial differential equation. By using spectral numerical methods in the spatial direction, and Matlab's ode45 solver in the time direction, we studied the numerical existence of steady-state and traveling wave solutions of the equation.

In particular, we found bifurcations values in terms of the diffusion parameter a for which new steady-state solutions emerge, and we determined the stability of each steady-state solution found. We were able to numerically estimate the speed of a traveling wave solution given the values of the growth rate and carrying capacity parameters. Finally we showed how a small Gaussian perturbation of the refuge level can lead to the steady-state outbreak level, and estimate how quickly that can happen.

References

[Aron et al. 2014] M. Aron, P. Bowers, N. Byer, R. Decker, A. Demirkaya, and J. H. Ryu, "Numerical results on existence and stability of steady state solutions for the reaction-diffusion and Klein–Gordon equations", *Involve* **7**:6 (2014), 723–742. MR Zbl

[Ludwig et al. 1978] D. Ludwig, D. D. Jones, and C. S. Holling, "Qualitative analysis of insect outbreak systems: the spruce budworm and forest", *J. Anim. Ecol.* **47**:1 (1978), 315–332.

[Murray 2005] J. Murray, *Mathematical biology, I: An introduction*, 3rd ed., Interdisciplinary applied mathematics **17**, Springer, New York, 2005. Zbl

[Seydel 2010] R. Seydel, *Practical bifurcation and stability analysis*, 3rd ed., Interdisciplinary Applied Mathematics **5**, Springer, 2010. MR Zbl

[Trefethen 2000] L. N. Trefethen, *Spectral methods in MATLAB*, Software, Environments, and Tools **10**, Society for Industrial and Applied Mathematics, Philadelphia, 2000. MR Zbl

[Williams and Birdsey 2003] D. W. Williams and R. A. Birdsey, "Historical patterns of spruce budworm defoliation and bark beetle outbreaks in North American conifer forests: an atlas and description of digital maps", general technical report NE-308, U.S. Department of Agriculture,

Forest Service, Northeastern Research Station, Newtown Square, PA, 2003, available at http://www.treesearch.fs.fed.us/pubs/5521.

alkhalil@stanford.edu   *Stanford University, Stanford, CA 94305, United States*

cbrenna1@ucsc.edu   *UC Santa Cruz, 1156 High Street, Santa Cruz, CA 95064, United States*

rdecker@hartford.edu   *Department of Mathematics, University of Hartford, 200 Bloomfield Ave, West Hartford, CT 06117, United States*

demirkaya@hartford.edu   *Department of Mathematics, University of Hartford, Dano Hall 210, 200 Bloomfield Ave, West Hartford, CT 06117, United States*

nagode@colostate.edu   *Colorado State University, Fort Collins, CO 80523, United States*

involve

msp.org/involve

INVOLVE YOUR STUDENTS IN RESEARCH

Involve showcases and encourages high-quality mathematical research involving students from all academic levels. The editorial board consists of mathematical scientists committed to nurturing student participation in research. Bridging the gap between the extremes of purely undergraduate research journals and mainstream research journals, *Involve* provides a venue to mathematicians wishing to encourage the creative involvement of students.

Cover: Alex Scorpan

© 2017 Mathematical Sciences Publishers

involve